IEEE Access
Multidisciplinary ⋮ Rapid Review ⋮ Open Access Journal

Received May 20, 2020, accepted June 8, 2020, date of publication June 24, 2020, date of current version July 8, 2020.

Digital Object Identifier 10.1109/ACCESS.2020.3004575

Multiple-Step Randomly Delayed Adaptive Robust Filter With Application to INS/VNS Integrated Navigation on Asteroid Missions

RONGJUN MU[1], BINGZHI SU[1], JIAYE CHEN[2], YUNTIAN LI[1], AND NAIGANG CUI[1]
[1]School of Astronautics, Harbin Institute of Technology, Harbin 150001, China
[2]Beijing Institute of Astronautical Systems Engineering, Beijing 100076, China

Corresponding author: Bingzhi Su (bingzhi_su_hit@hotmail.com)

This work was supported by the National Natural Science Foundation of China under Grant 61703125.

ABSTRACT This paper develops a novel nonlinear adaptive robust filter called the multiple-step randomly delayed variational Bayesian adaptive high-degree cubature Huber-based filter (MRD-VBAHCHF) for a class of nonlinear stochastic systems whose measurements are randomly delayed by multiple sampling times and corrupted by contaminated Gaussian noise with unknown covariance. First, a system with randomly delayed measurement is modeled in terms of multiple Bernoulli random variables. Then, the multiple-step randomly delayed high-degree cubature Kalman filter (MRD-HCKF) is derived by employing the fifth-degree cubature rule to compute the mean and covariance of the nonlinear equations in the system model. Next, the MRD-HCKF is modified to the MRD-VBAHCHF by incorporating the variational Bayesian theory and Huber technique for estimating the measurement noise covariance online and suppressing the influence of non-Gaussian noise. Consequently, the proposed filter is not only adaptive to unknown measurement noise statistics but also robust to random measurement delays and non-Gaussian noise. Finally, the MRD-VBAHCHF is verified for use in inertial navigation system/visual navigation system (INS/VNS) integrated navigation on asteroid missions, and the results of Monte Carlo simulations demonstrate that the MRD-VBAHCHF outperforms the high-degree cubature Kalman filter (HCKF), the MRD-HCKF and the variational Bayesian adaptive high-degree cubature Huber-based filter (VBAHCHF), thus showing the superiority of the proposed filter.

INDEX TERMS Randomly delayed measurements, adaptive robust filter, INS/VNS integrated navigation, asteroid missions.

I. INTRODUCTION

Asteroid exploration is significant for advancing our understanding of the Solar System and monitoring potential threats to the Earth. On future asteroid exploration missions, high-accuracy autonomous navigation will be an important foundation for guaranteeing the survival of the prospectors and completing the scheduled tasks. Inertial navigation systems (INSs) [1] and visual navigation systems (VNSs) [2] are two extensively used types of autonomous navigation systems for asteroid prospectors. An INS offers superior performance on a short time scale, but its navigation error drifts over time. By contrast, although a VNS can provide long-term accuracy in position and attitude by matching observations against a set of landmarks in an onboard database [2], its data update rate is infrequent because of the complexity of the corresponding image processing algorithm. Because of the complementary properties of INSs and VNSs, INS/VNS integrated navigation has been widely adopted for asteroid prospectors [3], [4]. The accuracy of INS/VNS integrated navigation strongly depends on the nonlinear filter used to fuse the data from the INS and VNS.

The most extensively used nonlinear filter for INS/VNS integrated navigation is the extended Kalman filter (EKF) [4], [5]. However, the performance of the EKF will be severely degraded for a system with strong nonlinearities because the EKF is based on first-order linearization [6]. Over the past few decades, several well-known Gaussian approximation filters have been developed based on deterministic sampling methods, such as the unscented Kalman filter (UKF) [7], [8], the cubature Kalman filter (CKF) [9], [10] and the Gauss-Hermite quadrature filter (GHQF) [11].

The associate editor coordinating the review of this manuscript and approving it for publication was Liang Hu.

The GHQF, which is based on a quadrature rule, can achieve better estimation accuracy than the UKF or CKF but suffers from the curse of dimensionality [12]. Recently, the arbitrary-degree cubature rule has been applied to develop the high-degree cubature Kalman filter (HCKF), which has a lower computational complexity than that of the GHQF [13].

However, it is worth pointing out that the abovementioned filters perform well only when three assumptions are satisfied: 1) the measurements arrive at the filter without any delay at every instant of time, 2) the measurement noise is subject to a Gaussian distribution, and 3) the statistical characteristics of the measurement noise are accurately known. However, in real-world applications, any of these assumptions may be violated since measurements are always randomly delayed due to unreliability in the transmission medium between the visual sensors and the filter [14] and are corrupted by contaminated Gaussian noise with unknown covariance arising from the complicated algorithmic image processing [15]–[17]. In this situation, the traditional Gaussian approximation filters perform poorly due to a lack of adaptivity and robustness.

To address the problem of estimation from measurements with random delay, various nonlinear filtering schemes, which make use of Bernoulli random variables to model the randomly delayed measurements, have been studied over the past decades. Hermoso-Carazo and Linares-Pérez proposed improved EKFs and UKFs for nonlinear systems in which the measurements are randomly delayed by one step [18] and two steps [19]. Later, by augmenting the states and the measurement noises, this work was generalized to a class of systems with multiple-step random measurement delays [20]–[22]. In [23], the multiple-step randomly delayed cubature Kalman filter (MRD-CKF), which uses the residuals and channel statistics of the received measurements to calculate tuned weighting factors, was proposed to handle nonlinear systems in the presence of multiple-step randomly delayed measurements. However, these studies ignored the presence of contaminated Gaussian measurement noise with unknown covariance, which may cause the filter accuracy to deteriorate. To tackle non-Gaussian measurement noise, Huber proposed a generalized likelihood technique [24] that is a hybrid of the l_1 and l_2 norm estimation techniques [25]. The Huber technique exhibits robustness with respect to contaminated Gaussian noise since it behaves both as an l_1 norm estimator for large residuals to reduce the impact of perturbing noise and as an l_2 norm estimator for small residuals to ensure both quality and efficiency in the case of a Gaussian distribution [26]. For the estimation problem under measurement noise with unknown statistics, variational Bayesian (VB) theory has been combined with a Gaussian filter to estimate the measurement noise covariance along with the system state and adaptively adjust the state-space model [16], [27]. Furthermore, the Huber technique has been embedded into VB theory to achieve both adaptivity and robustness through the Gaussian-Newton method [28], [29].

To overcome the aforementioned challenges, we propose a novel multiple-step randomly delayed variational Bayesian adaptive high-degree cubature Huber-based filter (MRD-VBAHCHF) in this paper. The prediction is derived based on a combination of the fifth-degree cubature rule, a multiple-step randomly delayed system model and VB theory. The update process is developed by modifying the conventional VB adaptive filter with the Huber technique. The main contribution of our paper is the proposal of a high-accuracy nonlinear filter with strong adaptivity and robustness; we not only consider multiple-step random delays in the received measurements but also account for the non-Gaussianity and covariance uncertainty of the measurement noise.

This paper is organized as follows. Section II formally defines and lays the analytical foundations for the considered problem. In section III, the multiple-step randomly delayed high-degree cubature filter (MRD-HCKF) is presented. In section IV, the MRD-HCKF is combined with the VB theory and Huber technique to derive the proposed MRD-VBAHCHF. Section V introduces a typical INS/VNS integrated navigation system used on asteroid missions. Section VI proves the superiority of the proposed filter on the basis of comparative simulations, and conclusions are drawn in section VII.

II. PROBLEM STATEMENT AND PRELIMINARIES

The nonlinear discrete-time stochastic system considered in this paper is described by [30]

$$\boldsymbol{x}_k = \boldsymbol{f}(\boldsymbol{x}_{k-1}) + \boldsymbol{w}_{k-1} \tag{1}$$

$$\boldsymbol{z}_k = \boldsymbol{h}(\boldsymbol{x}_k) + \boldsymbol{v}_k \tag{2}$$

where $\boldsymbol{x}_k \in \mathbb{R}^n$ is the state vector; m $\boldsymbol{z}_k \in \mathbb{R}^m$ is the measurement vector without delay; $\boldsymbol{f}(\boldsymbol{x}_{k-1})$ and $\boldsymbol{h}(\boldsymbol{x}_k)$ are the state function and measurement function, respectively, of the nonlinear system; $\boldsymbol{w}_{k-1} \in \mathbb{R}^n$ is the process noise, which is subject to a Gaussian distribution with zero mean and covariance $\boldsymbol{Q}_{k-1}$; $\boldsymbol{v}_k \in \mathbb{R}^m$ is the measurement noise; and the subscript k denotes the discrete time t_k.

A. MEASUREMENTS WITH MULTIPLE-STEP RANDOM DELAYS

In practice, visual measurements transferred to a processing center (filter) through an unreliable communication channel are always delayed. If the maximum transmission delay is d steps, then the measurements received by the filter at the kth time instant may be $\boldsymbol{z}_{k-i}$ $(0 \leqslant i \leqslant d)$. Therefore, the measurement equation in (2) should be rewritten as follows:

$$\begin{aligned}\boldsymbol{y}_k &= (1-\tau_1)\boldsymbol{z}_k + \tau_1(1-\tau_2)\boldsymbol{z}_{k-1} + \tau_1\tau_2(1-\tau_3)\boldsymbol{z}_{k-2} \\ &\quad \ldots + \left(\prod_{s=1}^{d-1}\tau_s\right)(1-\tau_d)\boldsymbol{z}_{k-d+1} + \Big[1-(1-\tau_1) \\ &\quad -\tau_1(1-\tau_2) - \cdots - \left(\prod_{s=1}^{d-1}\tau_s\right)(1-\tau_d)\Big]\boldsymbol{z}_{k-d} \\ &= \sum_{s=0}^{d}\tau^{(s,j)}\boldsymbol{z}_{k-s}\end{aligned} \tag{3}$$

where $\boldsymbol{y}_k$ is the measurement actually received by the filter; $\tau_0 = 1$; each τ_i $(i = 1, \ldots, d)$ is an independent Bernoulli random variable taking a value of either 0 or 1, with corresponding probabilities of $p(\tau_i = 1) = E[\tau_i] = p_i$ and $p(\tau_i = 0) = 1 - p_i$; and $\tau^{(s,j)}$ is given as follows:

$$\tau^{(s,j)} = \begin{cases} \left(\prod_{j=0}^{s} \tau_j\right)(1 - \tau_{s+1}), & 0 \leqslant s \leqslant d-1 \\ \prod_{j=0}^{d} \tau_j, & s = d \end{cases} \tag{4}$$

where only one of $\tau^{(s,j)}$ $(s = 0, 1, \ldots, d)$ takes value 1 and the others take value 0. This means that $\boldsymbol{y}_k$ may be one of $\{\boldsymbol{z}_{k-s}\}_{s=0}^{d}$.

The probability that a measurement is delayed by s $(0 \leqslant s \leqslant d)$ steps can be given as follows [22]:

$$p^{(s,j)} = \left(\prod_{j=0}^{s} p_j\right)(1 - p_{s+1}), \quad s = 0, 1, 2 \ldots, d-1 \tag{5}$$

$$p^{(d,j)} = \prod_{j=0}^{d} p_j \tag{6}$$

B. CONTAMINATED GAUSSIAN NOISE WITH UNKNOWN COVARIANCE IN SENSOR MEASUREMENTS

Sensor noise is often assumed to follow a Gaussian distribution with known statistical characteristics. However, not all real-word noise satisfies the above assumption. In particular, the noise of the visual sensor on an asteroid prospector is usually assumed to be contaminated Gaussian noise drawn from a Gaussian mixture distribution, and the probability density function can be expressed as follows [25], [28]:

$$p(\boldsymbol{v}) = (1 - \alpha)\mathrm{N}(\boldsymbol{v}; 0, \boldsymbol{R}_{sen}) + \alpha \mathrm{N}(\boldsymbol{v}; 0, \boldsymbol{R}_{per}) \tag{7}$$

where $\mathrm{N}(\boldsymbol{v}; 0, \boldsymbol{R}_{sen})$ is an ideal Gaussian distribution with unknown covariance $\boldsymbol{R}_{sen}$, $\mathrm{N}(\boldsymbol{v}; 0, \boldsymbol{R}_{per})$ is the perturbing Gaussian distribution, $\boldsymbol{v}$ is the vector of the sensor measurement noise, and α is the perturbing parameter, which represents the error model contamination.

III. MULTIPLE-STEP RANDOMLY DELAYED HIGH-DEGREE CUBATURE KALMAN FILTER

In this section, motivated by the superior performance of the HCKF in dealing with nonlinear systems, the MRD-HCKF is derived based on [23].

A. STATE AUGMENTATION

Considering (2) and (3), the measurement $\boldsymbol{y}_k$ that is actually available to the filter is a mixture of $\{\boldsymbol{z}_{k-s}\}_{s=0}^{d}$; hence, $\boldsymbol{y}_k$ depends on $\boldsymbol{x}_k, \boldsymbol{x}_{k-1}, \ldots, \boldsymbol{x}_{k-d}$. Therefore, the current state needs to be augmented with the previous states $\boldsymbol{x}_{k-1}, \boldsymbol{x}_{k-2}, \ldots, \boldsymbol{x}_{k-d}$. The augmented state can be expressed as

$$\boldsymbol{X}_k = \begin{bmatrix} \boldsymbol{x}_k \\ \boldsymbol{x}_{k-1} \\ \vdots \\ \boldsymbol{x}_{k-d} \end{bmatrix}_{n_a \times 1} \tag{8}$$

where $n_a = (d+1)n$ is the dimensionality of the augmented state vector.

The corresponding augmented system is

$$\boldsymbol{X}_k = \boldsymbol{F}(\boldsymbol{X}_{k-1}) + \boldsymbol{C}\boldsymbol{w}_{k-1} \tag{9}$$

$$\boldsymbol{y}_k = \boldsymbol{z}_{k-s} = \boldsymbol{h}(\boldsymbol{D}_s \boldsymbol{X}_k) + \boldsymbol{v}_{k-s}, \quad s = 0, 1, \ldots, d \tag{10}$$

where $\boldsymbol{F}(\boldsymbol{X}_{k-1})$, $\boldsymbol{C}$ and $\boldsymbol{D}_s\boldsymbol{X}_k$ are given as follows:

$$\boldsymbol{F}(\boldsymbol{X}_{k-1}) = \left[\boldsymbol{f}^T(\boldsymbol{x}_{k-1}), \boldsymbol{x}_{k-1}^T, \ldots, \boldsymbol{x}_{k-d}^T\right]^T \tag{11}$$

$$\boldsymbol{C} = [\boldsymbol{I}_{n\times n}, 0, \ldots, 0]^T \tag{12}$$

$$\boldsymbol{D}_s\boldsymbol{X}_k = \boldsymbol{x}_{k-s}, \quad s = 0, 1, 2, \ldots, d \tag{13}$$

B. PREDICTION

According to (8), the state estimate $\hat{\boldsymbol{X}}_{k-1/k-1}$ and the corresponding covariance $\boldsymbol{P}_{k-1/k-1}$ given $\boldsymbol{y}_{1:k-1}$ can be expressed as (14), shown at the bottom of the next page.

Then, the state prediction $\hat{\boldsymbol{X}}_{k/k-1}$ and the covariance $\boldsymbol{P}_{k/k-1}$ are given by

$$\hat{\boldsymbol{X}}_{k/k-1} = \begin{bmatrix} \hat{\boldsymbol{x}}_{k/k-1} \\ \hat{\boldsymbol{x}}_{k-1/k-1} \\ \vdots \\ \hat{\boldsymbol{x}}_{k-d/k-1} \end{bmatrix}$$

$$\boldsymbol{P}_{k/k-1} = \begin{bmatrix} \boldsymbol{P}^{xx}_{k,k/k-1} & \boldsymbol{P}^{xx}_{k,k-1/k-1} & \cdots & \boldsymbol{P}^{xx}_{k,k-d/k-1} \\ \boldsymbol{P}^{xx}_{k-1,k/k-1} & \boldsymbol{P}^{xx}_{k-1,k-1/k-1} & \cdots & \boldsymbol{P}^{xx}_{k-1,k-d/k-1} \\ \vdots & \vdots & \ddots & \vdots \\ \boldsymbol{P}^{xx}_{k-d,k/k-1} & \boldsymbol{P}^{xx}_{k-d,k-1/k-1} & \cdots & \boldsymbol{P}^{xx}_{k-d,k-d/k-1} \end{bmatrix} \tag{15}$$

It is clear that most of the block-matrix quantities in (15) can be obtained from (14), with the exceptions of $\hat{\boldsymbol{x}}_{k/k-1}$, $\boldsymbol{P}^{xx}_{k,k/k-1}$, $\{\boldsymbol{P}^{xx}_{k,k-s/k-1}\}_{s=1}^{d}$ and $\{\boldsymbol{P}^{xx}_{k-s,k/k-1}\}_{s=1}^{d}$, which are calculated as follows.

The fifth-degree cubature rule is utilized to calculate the Gaussian weighted integrals. The initial cubature point set is constructed on the basis of the state estimate $\hat{\boldsymbol{X}}_{k-1/k-1}$, the covariance $\boldsymbol{P}_{k-1/k-1}$ and the cubature point set $\boldsymbol{\Upsilon}$:

$$\boldsymbol{\chi}_{i,k-1/k-1} = \begin{bmatrix} \boldsymbol{\chi}^x_{i,k-1/k-1} \\ \vdots \\ \boldsymbol{\chi}^x_{i,k-d/k-1} \\ \boldsymbol{\chi}^x_{i,k-d-1/k-1} \end{bmatrix} = \sqrt{\boldsymbol{P}_{k-1/k-1}}\boldsymbol{\Upsilon}_i + \hat{\boldsymbol{X}}_{k-1/k-1} \quad i = 0, 1, 2 \ldots, 2n_a^2 \tag{16}$$

$$\boldsymbol{\Upsilon}_i = \begin{cases} [0,0,\ldots,0]^T & i=0 \\ \lambda \boldsymbol{s}_i^+ & i=1,2,\ldots,n_a(n_a-1)/2 \\ -\lambda \boldsymbol{s}_{i-n_a(n_a-1)/2}^+ & i=n_a(n_a-1)/2+1,\ldots,n_a(n_a-1) \\ \lambda \boldsymbol{s}_{i-n_a(n_a-1)}^- & i=n_a(n_a-1)+1,\ldots,\dfrac{3n_a(n_a-1)}{2} \\ -\lambda \boldsymbol{s}_{i-3n_a(n_a-1)/2}^- & i=\dfrac{3n_a(n_a-1)}{2}+1,\ldots,2n_a(n_a-1) \\ \lambda \boldsymbol{e}_{i-2n_a(n_a-1)} & i=2n_a(n_a-1)+1,\ldots,n(2n_a-1) \\ -\lambda \boldsymbol{e}_{i-n_a(2n_a-1)} & i=n_a(2n_a-1)+1,\ldots,2n_a^2 \end{cases} \tag{17}$$

where $\boldsymbol{e}_i \in \mathbb{R}^{n_a}$ is a unit vector, with the ith element being 1; $\lambda = \sqrt{n_a+2}$; and the vectors $\boldsymbol{s}_j^+$ and $\boldsymbol{s}_j^-$ are given by

$$\begin{aligned} \{\boldsymbol{s}_j^+\} &= \left\{ \sqrt{1/2}\left(\boldsymbol{e}_p + \boldsymbol{e}_q\right) : p<q; p,q=1,2,\cdots n_a \right\} \\ \{\boldsymbol{s}_j^-\} &= \left\{ \sqrt{1/2}\left(\boldsymbol{e}_p - \boldsymbol{e}_q\right) : p<q; p,q=1,2,\ldots n_a \right\} \end{aligned} \tag{18}$$

where the subscript j is given by

$$\begin{cases} j=1 & p=1,q=2 \\ j=\dfrac{(q-1)(q-2)}{2}+p & p<q,q>2 \end{cases} \tag{19}$$

Next, the state prediction $\hat{\boldsymbol{x}}_{k/k-1}$, the covariance $\boldsymbol{P}_{k,k/k-1}^{xx}$, and the cross-covariances $\boldsymbol{P}_{k,k-s/k-1}^{xx}$ and $\boldsymbol{P}_{k-s,k/k-1}^{xx}$ are calculated as follows:

$$\hat{\boldsymbol{x}}_{k/k-1} = \sum_{i=0}^{2n_a^2} \omega_i \boldsymbol{f}(\boldsymbol{\chi}_{i,k-1/k-1}^x) \tag{20}$$

$$\begin{aligned} \boldsymbol{P}_{k,k/k-1}^{xx} = &\sum_{i=0}^{2n_a^2} \omega_i \left(\boldsymbol{f}(\boldsymbol{\chi}_{i,k-1/k-1}^x) - \hat{\boldsymbol{x}}_{k/k-1}\right) \\ &\times \left(\boldsymbol{f}(\boldsymbol{\chi}_{i,k-1/k-1}^x) - \hat{\boldsymbol{x}}_{k/k-1}\right)^T + \boldsymbol{Q}_{k-1} \end{aligned} \tag{21}$$

$$\begin{aligned} \boldsymbol{P}_{k,k-s/k-1}^{xx} = &\sum_{i=0}^{2n_a^2} \omega_i \left(\boldsymbol{f}(\boldsymbol{\chi}_{i,k-1/k-1}^x) - \hat{\boldsymbol{x}}_{k/k-1}\right) \\ &\times \left(\boldsymbol{\chi}_{i,k-s/k-1}^x - \hat{\boldsymbol{x}}_{k-s/k-1}\right)^T,\ s=1,2,\ldots,d \end{aligned} \tag{22}$$

$$\boldsymbol{P}_{k-s,k/k-1}^{xx} = \left(\boldsymbol{P}_{k,k-s/k-1}^{xx}\right)^T, \quad s=1,2,\ldots,d \tag{23}$$

where the ω_i are weights given by

$$\omega_i = \begin{cases} \dfrac{2}{n_a+2} & i=0 \\ \dfrac{1}{(n_a+2)^2} & i=1,2,\ldots,2n_a(n_a-1) \\ \dfrac{(4-n_a)}{2(n_a+2)^2} & i=2n_a(n_a-1)+1,\ldots,2n_a^2 \end{cases} \tag{24}$$

By substituting (20)-(23) into (15), we can get the state prediction $\hat{\boldsymbol{X}}_{k/k-1}$ and the covariance $\boldsymbol{P}_{k/k-1}$.

Based on the state prediction $\hat{\boldsymbol{X}}_{k/k-1}$, the covariance $\boldsymbol{P}_{k/k-1}$ and the cubature point set $\boldsymbol{\Upsilon}$, we then generate the cubature points for the prediction step as follows:

$$\begin{aligned} \boldsymbol{\chi}_{i,k/k-1} &= \begin{bmatrix} \boldsymbol{\chi}_{i,k/k-1}^x \\ \vdots \\ \boldsymbol{\chi}_{i,k-d+1/k-1}^x \\ \boldsymbol{\chi}_{i,k-d/k-1}^x \end{bmatrix} \\ &= \sqrt{\boldsymbol{P}_{k/k-1}}\boldsymbol{\Upsilon}_i + \hat{\boldsymbol{X}}_{k/k-1}\ i=0,1,2\ldots,2n_a^2 \end{aligned} \tag{25}$$

The s-step-delayed measurement prediction $\hat{\boldsymbol{y}}_{k/k-1}^s$, the covariance $\boldsymbol{P}_{k/k-1}^{yy,s}$, the cross-covariance $\boldsymbol{P}_{k/k-1}^{Xy,s}$ and the filter gain $\boldsymbol{K}_k^s$ are calculated as shown below:

$$\hat{\boldsymbol{y}}_{k/k-1}^s = \sum_{i=0}^{2n_a^2} \omega_i \boldsymbol{h}(\boldsymbol{D}_s \boldsymbol{\chi}_{i,k/k-1}) \tag{26}$$

$$\begin{aligned} \boldsymbol{P}_{k/k-1}^{yy,s} = &\sum_{i=0}^{2n_a^2} \omega_i \left(\boldsymbol{h}(\boldsymbol{D}_s \boldsymbol{\chi}_{i,k/k-1}) - \hat{\boldsymbol{y}}_{k/k-1}^s\right) \\ &\times \left(\boldsymbol{h}(\boldsymbol{D}_s \boldsymbol{\chi}_{i,k/k-1}) - \hat{\boldsymbol{y}}_{k/k-1}^s\right)^T \end{aligned} \tag{27}$$

$$\begin{aligned} \boldsymbol{P}_{k/k-1}^{Xy,s} = &\sum_{i=0}^{2n_a^2} \omega_i \left(\boldsymbol{\chi}_{i,k/k-1} - \hat{\boldsymbol{X}}_{k/k-1}\right) \\ &\times \left(\boldsymbol{h}(\boldsymbol{D}_s \boldsymbol{\chi}_{i,k/k-1}) - \hat{\boldsymbol{y}}_{k/k-1}^s\right)^T \end{aligned} \tag{28}$$

$$\boldsymbol{K}_k^s = \boldsymbol{P}_{k/k-1}^{Xy,s}\left(\boldsymbol{P}_{k/k-1}^{yy,s} + \boldsymbol{R}_{k-s}\right)^{-1} \tag{29}$$

C. UPDATE

This subsection describes the process of updating the state and covariance based on a newly received measurement $\boldsymbol{y}_k$.

$$\hat{\boldsymbol{X}}_{k-1/k-1} = \begin{bmatrix} \hat{\boldsymbol{x}}_{k-1/k-1} \\ \vdots \\ \hat{\boldsymbol{x}}_{k-d/k-1} \\ \hat{\boldsymbol{x}}_{k-d-1/k-1} \end{bmatrix}$$

$$\boldsymbol{P}_{k-1/k-1} = \begin{bmatrix} \boldsymbol{P}_{k-1,k-1/k-1}^{xx} & \cdots & \boldsymbol{P}_{k-1,k-d/k-1}^{xx} & \boldsymbol{P}_{k-1,k-d-1/k-1}^{xx} \\ \vdots & \ddots & \vdots & \vdots \\ \boldsymbol{P}_{k-d,k-1/k-1}^{xx} & \cdots & \boldsymbol{P}_{k-d,k-d/k-1}^{xx} & \boldsymbol{P}_{k-d,k-d-1/k-1}^{xx} \\ \boldsymbol{P}_{k-d-1,k-1/k-1}^{xx} & \cdots & \boldsymbol{P}_{k-d-1,k-d/k-1}^{xx} & \boldsymbol{P}_{k-d-1,k-d-1/k-1}^{xx} \end{bmatrix} \tag{14}$$

Because the measurement $\boldsymbol{y}_k$ received from the sensor is a mixture of $\{z_{k-s}\}_{s=0}^{d}$, the measurement prediction is similarly a mixture of $\{\hat{\boldsymbol{y}}_{k/k-1}^{s}\}_{s=0}^{d}$. Similar to interacting multiple model (IMM) filter theory [23], [31], the update process consists of $d+1$ subupdates and is implemented by performing the following two steps.

1) CALCULATION OF THE sth SUBUPDATE

The newly received measurement $\boldsymbol{y}_k$ and the s-step-delayed measurement prediction $\hat{\boldsymbol{y}}_{k/k-1}^{s}$ $(0 \leqslant s \leqslant d)$ are used to update $\hat{\boldsymbol{X}}_{k/k}^{s}$ and $\boldsymbol{P}_{k/k}^{s}$:

$$\hat{\boldsymbol{X}}_{k/k}^{s} = \hat{\boldsymbol{X}}_{k/k-1} + \boldsymbol{K}_k^s \left(\boldsymbol{y}_k - \hat{\boldsymbol{y}}_{k/k-1}^{s}\right), \quad s = 0, 1, 2, \ldots, d \tag{30}$$

$$\boldsymbol{P}_{k/k}^{s} = \boldsymbol{P}_{k/k-1} - \boldsymbol{K}_k^s \left(\boldsymbol{P}_{k/k-1}^{Xy,s}\right)^T, \quad s = 0, 1, 2, \ldots, d \tag{31}$$

2) UPDATE INTEGRATION

The subupdate results $\hat{\boldsymbol{X}}_{k/k}^{s}$ and $\boldsymbol{P}_{k/k}^{s}$ are weighted to obtain the state estimate $\hat{\boldsymbol{X}}_{k/k}$ and its corresponding covariance $\boldsymbol{P}_{k/k}$, respectively:

$$\hat{\boldsymbol{X}}_{k/k} = \sum_{s=0}^{d} \mu_k^s \hat{\boldsymbol{X}}_{k/k}^{s} \tag{32}$$

$$\boldsymbol{P}_{k/k} = \sum_{s=0}^{d} \mu_k^s \boldsymbol{P}_{k/k}^{s} \tag{33}$$

where μ_k^s is a tunable weight that is calculated as shown in (34) based on residuals and delay probabilities.

$$\mu_k^s = \frac{p^{(s,j)} \mathrm{N}(\boldsymbol{y}_k; \hat{\boldsymbol{y}}_{k/k-1}^{s}, \boldsymbol{P}_{k/k-1}^{yy,s} + \boldsymbol{R}_{k-s})}{\sum_{i=0}^{d} \left[p^{(i,j)} \mathrm{N}(\boldsymbol{y}_k; \hat{\boldsymbol{y}}_{k/k-1}^{i}, \boldsymbol{P}_{k/k-1}^{yy,i} + \boldsymbol{R}_{k-i})\right]} \tag{34}$$

Remark 1: Although the structure of the MRD-HCKF is similar to that of the IMM filter, there are two main differences between them. First, every subfilter of the IMM filter yields its own prediction, whereas the MRD-HCKF produces only one prediction. Second, in the IMM filter, the model transition probability μ_k^s is updated on the basis of residuals, model transition probabilities and μ_{k-1}^s , whereas in the MRD-HCKF, it is calculated on the basis of residuals and delay probabilities.

IV. MULTIPLE-STEP RANDOMLY DELAYED VARIATIONAL BAYESIAN ADAPTIVE HIGH-DEGREE CUBATURE HUBER-BASED FILTER

To improve the adaptivity and robustness of the MRD-HCKF when faced with contaminated Gaussian noise with unknown covariance, the VB theory and Huber technique are incorporated into the MRD-HCKF to derive the novel MRD-VBAHCHF, which can estimate the unknown covariance of the measurement noise and suppress the influence of non-Gaussian noise. Similar to that of the MRD-HCKF, the update process of the MRD-VBAHCHF also consists of $d+1$ subupdates, where the state update is implemented in all subupdates, while the measurement noise covariance update is implemented only in the zeroth subupdate.

A. JOINT ESTIMATION OF THE STATE AND MEASUREMENT NOISE COVARIANCE USING VB THEORY

1) PREDICTION

The joint distribution of $\boldsymbol{X}_{k-1}$ and $\boldsymbol{R}_{k-1}$ given $\boldsymbol{y}_{1:k-1}$ can be approximated by the following factorized free form distribution:

$$\begin{aligned} p(\boldsymbol{X}_{k-1}, \boldsymbol{R}_{k-1} | \boldsymbol{y}_{1:k-1}) &= p(\boldsymbol{X}_{k-1} | \boldsymbol{y}_{1:k-1}) p(\boldsymbol{R}_{k-1} | \boldsymbol{y}_{1:k-1}) \\ &= \mathrm{N}(\boldsymbol{X}_{k-1}; \hat{\boldsymbol{X}}_{k-1/k-1}, \boldsymbol{P}_{k-1/k-1}) \\ &\quad \times IW(\boldsymbol{R}_{k-1}; \hat{u}_{k-1/k-1}, \hat{\boldsymbol{U}}_{k-1/k-1}) \end{aligned} \tag{35}$$

where $\mathrm{N}(\boldsymbol{X}_k; \boldsymbol{m}_k, \boldsymbol{P}_k)$ is a Gaussian distribution with mean $\boldsymbol{m}_k$ and covariance $\boldsymbol{P}_k$ and $\mathrm{IW}(\boldsymbol{R}_k; u_k, \boldsymbol{U}_k)$ is an inverse Wishart (IW) distribution governed by the degree-of-freedom parameter $u_k \in \mathbb{R}$ and the scale matrix $\boldsymbol{U}_k \in \mathbb{R}^{m \times m}$ for the measurement noise covariance $\boldsymbol{R}_k$.

Because the IW distribution is a conjugate prior distribution for the covariance of the Gaussian distribution, the joint predicted distribution can be expressed as the following Gaussian-IW distribution:

$$\begin{aligned} p(\boldsymbol{X}_k, \boldsymbol{R}_k | \boldsymbol{y}_{1:k-1}) &= p(\boldsymbol{X}_k | \boldsymbol{y}_{1:k-1}) p(\boldsymbol{R}_k | \boldsymbol{y}_{1:k-1}) \\ &= \mathrm{N}(\boldsymbol{X}_k; \hat{\boldsymbol{X}}_{k/k-1}, \boldsymbol{P}_{k/k-1}) \\ &\quad \times \mathrm{IW}(\boldsymbol{R}_k; \hat{u}_{k/k-1}, \hat{\boldsymbol{U}}_{k/k-1}) \end{aligned} \tag{36}$$

where the state prediction $\hat{\boldsymbol{X}}_{k/k-1}$ and the covariance $\boldsymbol{P}_{k/k-1}$ can be obtained from (15) and $\hat{u}_{k/k-1}$ and $\hat{\boldsymbol{U}}_{k/k-1}$ are given by

$$\hat{u}_{k/k-1} = \kappa(\hat{u}_{k-1/k-1} - m - 1) + m + 1 \tag{37}$$

$$\hat{\boldsymbol{U}}_{k/k-1} = \boldsymbol{B} \hat{\boldsymbol{U}}_{k-1/k-1} \boldsymbol{B}^T \tag{38}$$

where κ is a discount parameter satisfying $0 < \kappa \leqslant 1$ and the matrix $\boldsymbol{B} = \sqrt{\kappa} \boldsymbol{I}_{m \times m}$ is chosen to guarantee that the form of the distribution of the measurement noise covariance remains unchanged.

2) UPDATE

Next, to make the computation tractable, the joint posterior distribution $p(\boldsymbol{X}_k, \boldsymbol{R}_k | \boldsymbol{y}_{1:k})$ is formed by applying the VB approximation:

$$p(\boldsymbol{X}_k, \boldsymbol{R}_k | \boldsymbol{y}_{1:k}) \approx Q_x(\boldsymbol{X}_k) Q_R(\boldsymbol{R}_k) \tag{39}$$

where $Q_x(\boldsymbol{X}_k)$ and $Q_R(\boldsymbol{R}_k)$ are the unknown approximate densities for the state and measurement noise covariance, respectively.

By minimizing the Kullback–Leibler (KL) divergence with respect to the probability densities, we can obtain $Q_x(\boldsymbol{X}_k)$ and $Q_R(\boldsymbol{R}_k)$:

$$Q_X(\boldsymbol{X}_k) \propto exp\left(\int \log p(\boldsymbol{y}_k, \boldsymbol{X}_k, \boldsymbol{R}_k | \boldsymbol{y}_{1:k-1}) Q_R(\boldsymbol{R}_k) d\boldsymbol{R}_k\right) \tag{40}$$

$$Q_R(\boldsymbol{R}_k) \propto exp\left(\int \log p(\boldsymbol{y}_k, \boldsymbol{X}_k, \boldsymbol{R}_k | \boldsymbol{y}_{1:k-1}) Q_X(\boldsymbol{X}_k) d\boldsymbol{X}_k\right) \tag{41}$$

Finally, the state update (42)-(44) and measurement noise covariance update (45)-(48) can be performed by comparing the integral terms in (40) and (41) with the Gaussian distribution and the IW distribution, respectively:

$$\boldsymbol{K}_k^0 = \boldsymbol{P}_{k/k-1}^{Xy,0}\left(\boldsymbol{P}_{k/k-1}^{yy,0} + \hat{\boldsymbol{R}}_k\right)^{-1} \tag{42}$$

$$\hat{\boldsymbol{X}}_{k/k}^0 = \hat{\boldsymbol{X}}_{k/k-1} + \boldsymbol{K}_k^0(\boldsymbol{y}_k - \hat{\boldsymbol{y}}_{k/k-1}^0) \tag{43}$$

$$\boldsymbol{P}_{k/k}^0 = \boldsymbol{P}_{k/k-1} - \boldsymbol{K}_k^0(\boldsymbol{P}_{k/k-1}^{Xz,0})^T \tag{44}$$

$$\boldsymbol{\chi}_{i,k/k}^0 = \sqrt{\boldsymbol{P}_{k/k}^0}\boldsymbol{\Upsilon}_i + \hat{\boldsymbol{X}}_{k/k}^0 \tag{45}$$

$$\hat{u}_{k/k} = \hat{u}_{k/k-1} + 1 \tag{46}$$

$$\hat{\boldsymbol{U}}_{k/k} = \hat{\boldsymbol{U}}_{k/k-1} + \mu_k^0 \sum_{i=0}^{2n_a^2} \omega_i \left(\boldsymbol{y}_k - \boldsymbol{h}(\boldsymbol{D}_0\boldsymbol{\chi}_{i,k/k}^0)\right) \times \left(\boldsymbol{y}_k - \boldsymbol{h}(\boldsymbol{D}_0\boldsymbol{\chi}_{i,k/k}^0)\right)^T \tag{47}$$

$$\hat{\boldsymbol{R}}_k = (\hat{u}_{k/k} - m - 1)^{-1}\hat{\boldsymbol{U}}_{k/k} \tag{48}$$

where the updated cubature point set based on $\hat{\boldsymbol{X}}_{k/k}^0$ and $\sqrt{\boldsymbol{P}_{k/k}^0}$ is given by

$$\boldsymbol{\chi}_{i,k/k}^0 = \begin{bmatrix} \boldsymbol{\chi}_{i,k/k}^{0,x} \\ \vdots \\ \boldsymbol{\chi}_{i,k-d+2/k-1}^{0,x} \\ \boldsymbol{\chi}_{i,k-d+1/k-1}^{0,x} \end{bmatrix} = \sqrt{\boldsymbol{P}_{k/k}^0}\boldsymbol{\Upsilon}_i + \hat{\boldsymbol{X}}_{k/k}^0, \ i = 0, 1, \ldots, 2n_a^2 \tag{49}$$

It can be seen that the state update and the measurement noise covariance update are coupled; hence, they should be solved by means of fixed-point iteration.

B. MODIFICATION OF THE UPDATE PROCESS USING THE HUBER TECHNIQUE

1) MODIFICATION OF THE STATE UPDATE

By defining the state prediction error and the measurement matrix as

$$\delta\boldsymbol{X}_k^s = \hat{\boldsymbol{X}}_{k/k-1} - \boldsymbol{X}_k^s, \quad s = 0, 1, 2, \ldots, d \tag{50}$$

$$\boldsymbol{H}_k^s = [(\boldsymbol{P}_{k/k-1})^{-1}\boldsymbol{P}_{k/k-1}^{Xy,s}]^T, \quad s = 0, 1, 2, \ldots, d \tag{51}$$

the state update can be recast as a linear regression problem:

$$\widehat{\boldsymbol{y}}_k^s = \boldsymbol{L}_k^s\boldsymbol{X}_k^s + \varsigma_k^s \tag{52}$$

where

$$\boldsymbol{T}_k^s = \begin{bmatrix} \hat{\boldsymbol{R}}_{k-s} & 0 \\ 0 & \boldsymbol{P}_{k/k-1} \end{bmatrix} \tag{53}$$

$$\widehat{\boldsymbol{y}}_k^s = (\boldsymbol{T}_k^s)^{-1/2}\begin{Bmatrix} \boldsymbol{y}_k - \hat{\boldsymbol{y}}_{k/k-1}^s + \boldsymbol{H}_k^s\hat{\boldsymbol{X}}_{k/k-1} \\ \hat{\boldsymbol{X}}_{k/k-1} \end{Bmatrix} \tag{54}$$

$$\boldsymbol{L}_k^s = (\boldsymbol{T}_k^s)^{-1/2}\begin{bmatrix} \boldsymbol{H}_k^s \\ \boldsymbol{I}_{n_a \times n_a} \end{bmatrix} \tag{55}$$

$$\varsigma_k^s = (\boldsymbol{T}_k^s)^{-1/2}\begin{Bmatrix} \boldsymbol{v}_{k-s} \\ \delta\boldsymbol{X}_k^s \end{Bmatrix} \tag{56}$$

Then, the linear regression problem can be solved by minimizing the following objective function:

$$J(\boldsymbol{X}_k^s) = \sum_{i=1}^{m+n_a} \ell(\xi_i^s) \tag{57}$$

where $\xi_i^s = (\boldsymbol{L}_k^s\hat{\boldsymbol{X}}_{k/k}^s - \widehat{\boldsymbol{y}}_k^s)_i$ is the ith component of the normalized residual vector and the real-valued function $\ell(\cdot)$ introduced by Huber is given by

$$\ell(\xi_i^s) = \begin{cases} \frac{1}{2}(\xi_i^s)^2 & |\xi_i^s| < \beta \\ \beta|\xi_i^s| - \frac{1}{2}\beta^2 & |\xi_i^s| \geqslant \beta \end{cases} \tag{58}$$

where β is a tuning parameter.

Taking the derivative of objective function (57) with respect to $\boldsymbol{X}_k^s$ yields

$$\sum_{i=1}^{m+n_a} \ell'(\xi_i^s)\frac{\partial\xi_i^s}{\partial\boldsymbol{X}_k^s} = 0 \tag{59}$$

where

$$\ell'(\xi_i^s) = \frac{d\ell(\xi_i^s)}{d\xi_i^s} \tag{60}$$

Equation (59) can be rewritten as follows:

$$(\boldsymbol{T}_k^s)^T\boldsymbol{\Phi}^s(\boldsymbol{T}_k^s\boldsymbol{X}_k^s - \widehat{\boldsymbol{y}}_k^s) = 0 \tag{61}$$

where

$$\boldsymbol{\Phi}^s = diag[\psi(\xi_i^s)] \tag{62}$$

$$\psi(\xi_i^s) = \frac{\ell'(\xi_i^s)}{\xi_i^s} \tag{63}$$

The iterative solution can be expressed as

$$\boldsymbol{X}_{k/k}^{s,(j)} = \left(\boldsymbol{\Phi}^{s,(j-1)}\boldsymbol{T}_k^s\right)^{-1}(\boldsymbol{T}_k^s)^T\boldsymbol{\Phi}^{s,(j-1)}\widehat{\boldsymbol{y}}_k^s \tag{64}$$

where the superscript j is the iteration index.

The covariance $\boldsymbol{P}_{k/k}^s$ is computed as

$$\boldsymbol{P}_{k/k}^s = \left((\boldsymbol{T}_k^s)^T\boldsymbol{\Phi}^s\boldsymbol{T}_k^s\right)^{-1} \tag{65}$$

$\boldsymbol{\Phi}^s$ in (62) can be decomposed into two components:

$$\boldsymbol{\Phi}^s = \begin{bmatrix} \boldsymbol{\Phi}_y^s & 0 \\ 0 & \boldsymbol{\Phi}_X^s \end{bmatrix} \tag{66}$$

where $\boldsymbol{\Phi}_y^s$ and $\boldsymbol{\Phi}_X^s$ correspond to the residuals of the measurement prediction and state prediction, respectively.

Finally, (64) and (65) can be rewritten in the following iteratively reweighted filter form:

$$\hat{\boldsymbol{X}}_{k/k}^{s,(j)} = \hat{\boldsymbol{X}}_{k/k-1} + \boldsymbol{K}_k^{s,(j-1)}\left[\boldsymbol{y}_k - \hat{\boldsymbol{y}}_{k/k-1}^s\right] \tag{67}$$

$$\boldsymbol{P}_{k/k}^{s,(j)} = \left(\boldsymbol{I} - \boldsymbol{K}_k^{s,(j-1)}\boldsymbol{H}_k^s\right)\boldsymbol{P}_{k/k-1}^{1/2}(\boldsymbol{\Phi}_X^{s,(j-1)})^{-1}\boldsymbol{P}_{k/k-1}^{1/2} \quad (68)$$

where the gain matrix is calculated as

$$\begin{aligned}&\boldsymbol{K}_k^{s,(j-1)}\\ &= \boldsymbol{P}_{k/k-1}^{1/2}(\boldsymbol{\Phi}_X^{s,(j-1)})^{-1}\boldsymbol{P}_{k/k-1}^{1/2}(\boldsymbol{H}_k^s)^T\left[\boldsymbol{H}_k^s\boldsymbol{P}_{k/k-1}^{1/2}\right.\\ &\quad\left.(\boldsymbol{\Phi}_X^{s,(j-1)})^{-1}\boldsymbol{P}_{k/k-1}^{1/2}(\boldsymbol{H}_k^s)^T + \hat{\boldsymbol{R}}_{k-s}^{1/2}(\boldsymbol{\Phi}_y^{s,(j-1)})^{-1}\hat{\boldsymbol{R}}_{k-s}^{1/2}\right]^{-1}\end{aligned} \quad (69)$$

2) MODIFICATION OF THE MEASUREMENT NOISE COVARIANCE UPDATE

To guarantee the estimation accuracy for the measurement noise covariance, according to [15], the measurement $\boldsymbol{y}_k$ corrupted by contaminated noise as expressed in (47) should be modified to

$$\breve{\boldsymbol{y}}_{k/k} = \hat{\boldsymbol{y}}_{k/k} + \boldsymbol{\Phi}_y\hat{\boldsymbol{R}}_k^{1/2}\xi^0(1:m,1) \quad (70)$$

where the measurement estimate $\hat{\boldsymbol{y}}_{k/k}$ is calculated as

$$\hat{\boldsymbol{y}}_{k/k} = \sum_{i=0}^{2n_a^2}\boldsymbol{h}(\boldsymbol{D}_0\boldsymbol{\chi}_{i,k/k}^0) \quad (71)$$

C. MRD-VBAHCHF ALGORITHM

Because the covariance $\hat{\boldsymbol{R}}_{k-s} = (\hat{u}_{k-s/k-s}-m-1)^{-1}\hat{\boldsymbol{U}}_{k-s/k-s}$ is used in the sth subupdate ($0 \leqslant s \leqslant d$), the degree-of-freedom parameter and the scale matrix must be augmented with the previous ones up to d steps back:

$$\boldsymbol{u}_k^a = \begin{bmatrix}u_k\\ u_{k-1}\\ \vdots\\ u_{k-d}\end{bmatrix}_{n_a\times 1}, \quad \boldsymbol{U}_k^a = \begin{bmatrix}\boldsymbol{U}_k\\ \boldsymbol{U}_{k-1}\\ \vdots\\ \boldsymbol{U}_{k-d}\end{bmatrix}_{n_u\times m} \quad (72)$$

where $n_u = n_a \times m$.

The augmented degree-of-freedom parameter $\hat{\boldsymbol{u}}_{k-1/k-1}^a$ and the augmented scale matrix $\hat{\boldsymbol{U}}_{k-1/k-1}^a$ given $\boldsymbol{y}_{1:k-1}$ can be expressed as

$$\begin{aligned}\hat{\boldsymbol{u}}_{k-1/k-1}^a &= \begin{bmatrix}\hat{u}_{k-1/k-1}\\ \hat{u}_{k-2/k-1}\\ \vdots\\ \hat{u}_{k-d-1/k-1}\end{bmatrix},\\ \hat{\boldsymbol{U}}_{k-1/k-1}^a &= \begin{bmatrix}\hat{\boldsymbol{U}}_{k-1/k-1}\\ \hat{\boldsymbol{U}}_{k-2/k-1}\\ \vdots\\ \hat{\boldsymbol{U}}_{k-d-1/k-1}\end{bmatrix}\end{aligned} \quad (73)$$

Then, $\hat{\boldsymbol{u}}_{k/k-1}^a$ and $\hat{\boldsymbol{U}}_{k/k-1}^a$ in the prediction step are given by

$$\hat{\boldsymbol{u}}_{k/k-1}^a = \begin{bmatrix}\hat{u}_{k/k-1}\\ \hat{u}_{k-1/k-1}\\ \vdots\\ \hat{u}_{k-d/k-1}\end{bmatrix}, \quad \hat{\boldsymbol{U}}_{k/k-1}^a = \begin{bmatrix}\hat{\boldsymbol{U}}_{k/k-1}\\ \hat{\boldsymbol{U}}_{k-1/k-1}\\ \vdots\\ \hat{\boldsymbol{U}}_{k-d/k-1}\end{bmatrix} \quad (74)$$

where $\hat{u}_{k/k-1}$ and $\hat{\boldsymbol{U}}_{k/k-1}$ can be obtained as shown in (37) and (38), and the other elements are given in (73).

Next, $\hat{\boldsymbol{u}}_{k/k}^a$ and $\hat{\boldsymbol{U}}_{k/k}^a$ can be updated as follows:

$$\hat{\boldsymbol{u}}_{k/k}^a = \begin{bmatrix}\hat{u}_{k/k}\\ \hat{u}_{k-1/k}\\ \vdots\\ \hat{u}_{k-d/k}\end{bmatrix}, \quad \hat{\boldsymbol{U}}_{k/k-1}^a = \begin{bmatrix}\hat{\boldsymbol{U}}_{k/k}\\ \hat{\boldsymbol{U}}_{k-1/k}\\ \vdots\\ \hat{\boldsymbol{U}}_{k-d/k}\end{bmatrix} \quad (75)$$

where $\hat{u}_{k/k}$ and $\hat{\boldsymbol{U}}_{k/k}$ can be obtained as shown in (46) and (47), and the other elements can be updated as follows:

$$\hat{u}_{k-s/k} = \hat{u}_{k-s/k-1}, \quad s = 1,2,\ldots,d \quad (76)$$

$$\hat{\boldsymbol{U}}_{k-s/k} = \hat{\boldsymbol{U}}_{k-s/k-1}, \quad s = 1,2,\ldots,d \quad (77)$$

Finally, to clearly illustrate the calculation process of the MRD-VBAHCHF, the main steps of the proposed filtering algorithm are summarized in Fig. 1.

V. INS/VNS INTEGRATED NAVIGATION

A. REFERENCE FRAME

To establish the INS/VNS integrated navigation system model, four coordinate frames are first defined. A sketch of the geometrical relationships among these reference frames is shown in Fig. 2.

1) ASTEROID-CENTERED ASTEROID-FIXED FRAME

It is assumed that the origin of the asteroid-centered asteroid-fixed frame (a frame) is located at the center of the asteroid and that the x_a axis, y_a axis and z_a axis are coincident with the minimum, intermediate and maximum inertia axes, respectively, of the asteroid. The a frame rotates together with the asteroid around the z_a axis.

2) ASTEROID-CENTERED INERTIAL FRAME

The definitions of the origin and axes of the asteroid-centered inertial frame (i frame) are the same as those for the a frame; however, the i frame remains unchanged in the inertial space.

3) PROSPECTOR BODY FRAME

The prospector body frame (b frame) is rigidly attached to the prospector, with its origin at the center of the prospector and the x_b axis, y_b axis and z_b axis being the principal inertial axes of the spacecraft. $\boldsymbol{C}_b^a$ is the matrix for the coordinate transformation from the b frame to the a frame and can be defined in terms of a 3-2-1 sequence of rotations as follows:

$$\begin{aligned}&\boldsymbol{C}_b^a\\ &= \left(\boldsymbol{C}_a^b\right)^T\\ &= \begin{bmatrix}\mathrm{c}\theta\,\mathrm{c}\phi & -s\phi\,\mathrm{c}\gamma + \mathrm{s}\theta\,\mathrm{c}\phi\,\mathrm{s}\gamma & \mathrm{s}\phi\,\mathrm{s}\gamma + \mathrm{s}\theta\,\mathrm{c}\phi\,\mathrm{c}\gamma\\ \mathrm{c}\theta\,\mathrm{s}\phi & c\phi\,\mathrm{c}\gamma + s\theta s\phi s\gamma & -\mathrm{c}\phi\,\mathrm{s}\gamma + \mathrm{s}\theta\,\mathrm{s}\phi\,\mathrm{c}\gamma\\ -\mathrm{s}\theta & c\theta\,\mathrm{s}\gamma & \mathrm{c}\theta\,\mathrm{c}\gamma\end{bmatrix}\end{aligned} \quad (78)$$

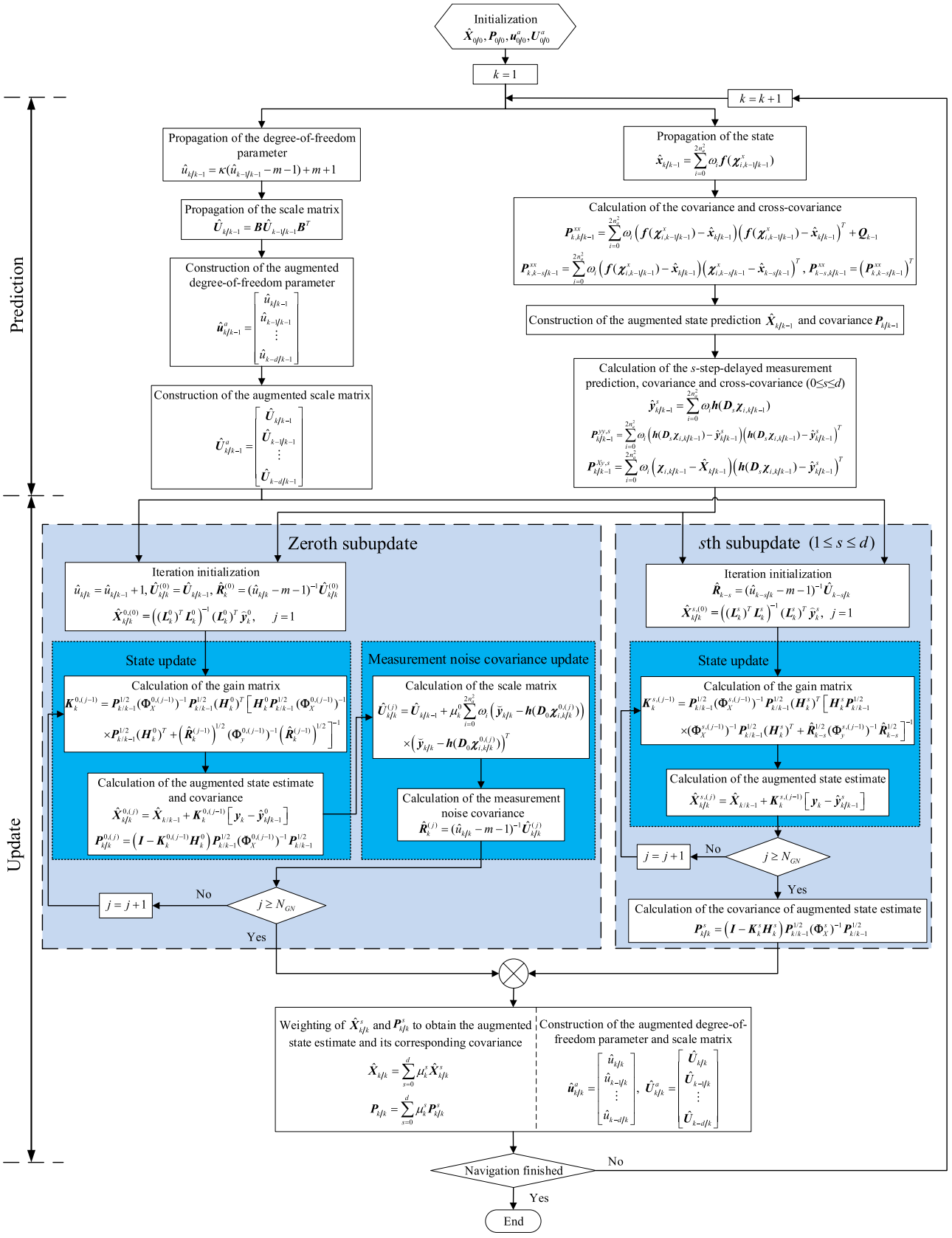

FIGURE 1. Flowchart of the MRD-VBAHCHF.

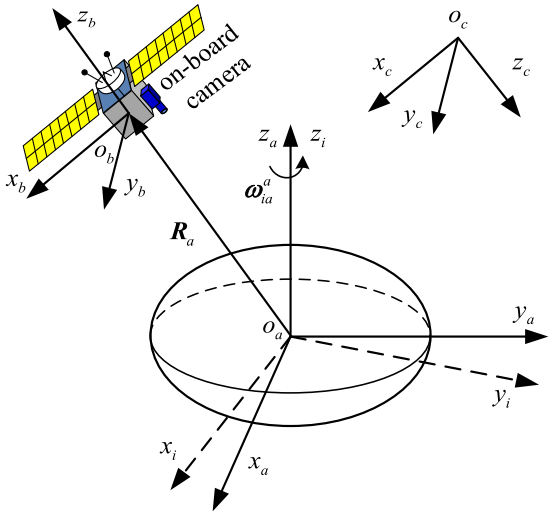

FIGURE 2. Sketch of the geometrical relationships among the reference frames.

where θ, ϕ and γ are the pitch angle, yaw angle and roll angle, respectively. In addition, the following notations are used: $\mathrm{c}\,\varphi \equiv \cos\varphi$, $\varphi = \theta, \phi, \gamma$ and $s\varphi \equiv \sin\varphi$.

4) CAMERA FRAME

Let the origin of the camera frame (c frame) lie at the optical center of the camera. The z_c axis is parallel to the optical axis of the lens, while the x_c axis and y_c axis lie within the image plane. The matrix $\boldsymbol{C}_b^c$ for the coordinate transformation from the b frame to the c frame is

$$\boldsymbol{C}_b^c = \begin{bmatrix} \cos\phi_c & 0 & -\sin\phi_c \\ \sin\theta_c \sin\phi_c & \cos\theta_c & \sin\theta_c \cos\phi_c \\ \cos\theta_c \sin\phi_c & -\sin\theta_c & \cos\theta_c \cos\phi_c \end{bmatrix} \tag{79}$$

where θ_c and ϕ_c are the camera installation angles.

B. INS/VNS INTEGRATED NAVIGATION MODEL

1) STATE MODEL

The mechanical model of the INS is chosen to be a state model. First, the state vector is defined as follows:

$$\boldsymbol{x}_k = \left[\boldsymbol{R}_a^T, \boldsymbol{V}_a^T, \boldsymbol{\Psi}^T, \boldsymbol{b}_a^T, \boldsymbol{b}_g^T\right]^T \tag{80}$$

where $\boldsymbol{R}_a = [x, y, z]^T$ and $\boldsymbol{V}_a = [v_x, v_y, v_z]^T$ represent the position and velocity, respectively, of the prospector in the a frame; $\boldsymbol{\Psi} = [\theta, \phi, \gamma]$ is the attitude; and $\boldsymbol{b}_a$ and $\boldsymbol{b}_g$ are the biases of the accelerometer and gyro, respectively, as defined in the b frame.

Then, the mechanical equations of the INS can be summarized as follows:

$$\dot{\boldsymbol{R}}_a = \boldsymbol{V}_a \tag{81}$$

$$\dot{\boldsymbol{V}}_a = \boldsymbol{C}_b^a\left(\tilde{\boldsymbol{a}}^b - \boldsymbol{b}_a - \boldsymbol{\nabla}_v\right) - 2\boldsymbol{\omega}_{ia}^a \times \boldsymbol{V}_a - \boldsymbol{\omega}_{ia}^a \times \boldsymbol{\omega}_{ia}^a \times \boldsymbol{R}_a + \boldsymbol{g}_a \tag{82}$$

$$\dot{\boldsymbol{\Psi}} = \boldsymbol{\Omega}(\boldsymbol{\Psi})\left(\tilde{\boldsymbol{\omega}}_{ib}^b - \boldsymbol{b}_g - \boldsymbol{\varepsilon}_v - \boldsymbol{C}_a^b \boldsymbol{\omega}_{ia}^a\right) \tag{83}$$

$$\dot{\boldsymbol{b}}_a = \boldsymbol{\nabla}_u \tag{84}$$

$$\dot{\boldsymbol{b}}_g = \boldsymbol{\varepsilon}_u \tag{85}$$

with

$$\boldsymbol{\Omega}(\boldsymbol{\Psi}) = \begin{bmatrix} 0 & \cos\gamma & -\sin\gamma \\ 0 & \dfrac{\mathrm{sos}\,\gamma}{\cos\theta} & \dfrac{\cos\gamma}{\cos\theta} \\ 1 & \tan\theta\sin\gamma & \tan\theta\cos\gamma \end{bmatrix} \tag{86}$$

where $\tilde{\boldsymbol{a}}^b$ is the accelerometer measurement; $\tilde{\boldsymbol{\omega}}_{ib}^b$ is the gyro measurement; $\boldsymbol{\nabla}_v$, $\boldsymbol{\nabla}_u$, $\boldsymbol{\varepsilon}_v$ and $\boldsymbol{\varepsilon}_u$ are zero-mean Gaussian white noise terms with spectral densities given by $\sigma_{av}^2\boldsymbol{I}_{3\times3}$, $\sigma_{au}^2\boldsymbol{I}_{3\times3}$, $\sigma_{gv}^2\boldsymbol{I}_{3\times3}$ and $\sigma_{gu}^2\boldsymbol{I}_{3\times3}$, respectively; $\boldsymbol{\omega}_{ia}^a$ is the spin rate of the asteroid in the a frame; and $\boldsymbol{g}_a$ is the gravitational vector represented in the a frame.

According to (81)-(85), the nonlinear state model of the INS/VNS integrated navigation system can be written in differential form as follows:

$$\begin{aligned} \dot{\boldsymbol{x}}_k &= \boldsymbol{f}(\boldsymbol{x}_{k-1}) + \boldsymbol{w}_k \\ &= \begin{bmatrix} \boldsymbol{V}_a \\ \boldsymbol{C}_b^a\left(\tilde{\boldsymbol{a}}^b - \boldsymbol{b}_a\right) - 2\boldsymbol{\omega}_{ia}^a \times \boldsymbol{V}_a - \boldsymbol{\omega}_{ia}^a \times \boldsymbol{\omega}_{ia}^a \times \boldsymbol{R}_a + \boldsymbol{g}_a \\ \boldsymbol{\Omega}(\boldsymbol{\Psi})\left(\tilde{\boldsymbol{\omega}}_{ib}^b - \boldsymbol{b}_g - \boldsymbol{C}_a^b\boldsymbol{\omega}_{ia}^a\right) \\ 0 \\ 0 \end{bmatrix} \\ &\quad + \begin{bmatrix} 0 \\ -\boldsymbol{C}_b^a\boldsymbol{\nabla}_v \\ -\boldsymbol{\Omega}(\boldsymbol{\Psi})\boldsymbol{\varepsilon}_v \\ \boldsymbol{\nabla}_u \\ \boldsymbol{\varepsilon}_u \end{bmatrix} \end{aligned} \tag{87}$$

2) MEASUREMENT MODEL

The measurements of the visual sensor are acquired along the lines of sight (LOSs) between the prospector and landmarks such as craters and rocks. A schematic of this system is shown in Fig. 3. The measurement equation for the visual sensor can be expressed as

$$\begin{aligned} \boldsymbol{z}_{k,j} &= \boldsymbol{h}_j(\boldsymbol{x}_k) + \boldsymbol{v}_{k,j} \\ &= \boldsymbol{C}_b^c\boldsymbol{C}_a^b \frac{1}{\sqrt{(x_{l,j}-x)^2 + (y_{l,j}-y)^2 + (z_{l,j}-z)^2}} \\ &\quad \times \begin{bmatrix} x_{l,j}-x \\ y_{l,j}-y \\ z_{l,j}-z \end{bmatrix} + \boldsymbol{v}_{k,j} \end{aligned} \tag{88}$$

where $\boldsymbol{R}_{l,j} = [x_{l,j}, y_{l,j}, z_{l,j}]^T$ represents the positions of landmarks, $\boldsymbol{z}_{k,j}$ indicate the measurement of the jth feature at time k.

The VNS can determine the attitude and position of the prospector using three LOS vectors [32]. The corresponding navigation accuracy is affected by the geometry between the matched landmark features and the prospector, in a manner similar to the dilution of precision (DOP) in a global navigation satellite system [33]. Thus, the measurement model

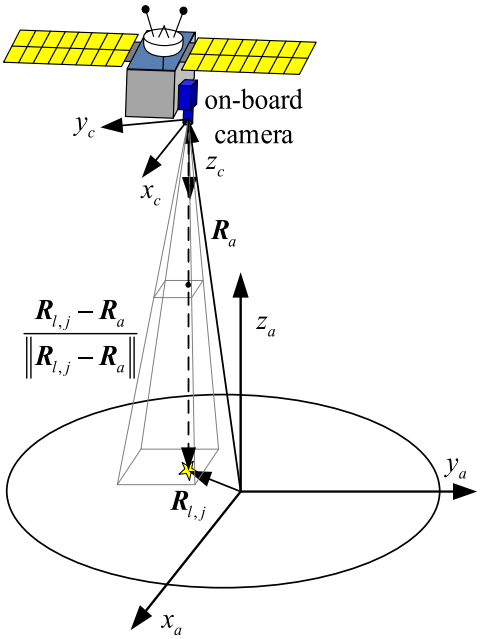

FIGURE 3. Visual navigation system.

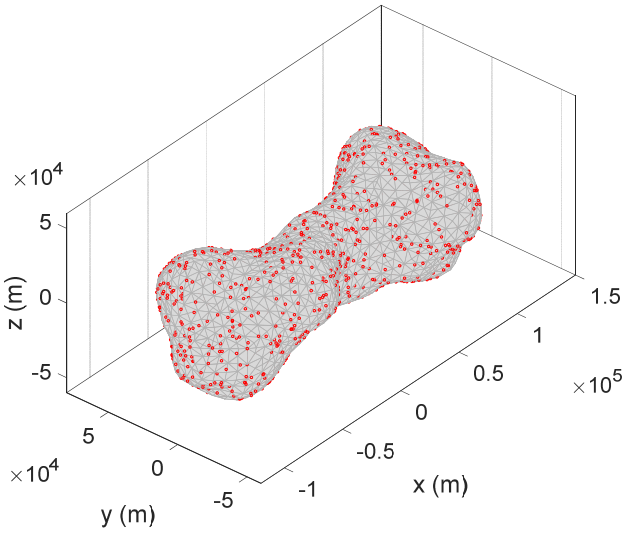

FIGURE 4. Asteroid Kleopatra, with 1250 landmarks.

based on three features selected on the basis of the position DOP can be formulated as follows:

$$z_k = \boldsymbol{h}(\boldsymbol{x}_k) + \boldsymbol{v}_k = \begin{bmatrix} \boldsymbol{h}_1(\boldsymbol{x}_k) \\ \boldsymbol{h}_2(\boldsymbol{x}_k) \\ \boldsymbol{h}_3(\boldsymbol{x}_k) \end{bmatrix} + \begin{bmatrix} \boldsymbol{v}_{k,1} \\ \boldsymbol{v}_{k,2} \\ \boldsymbol{v}_{k,3} \end{bmatrix} \tag{89}$$

VI. SIMULATIONS

Simulations were conducted to validate the superior filtering performance of the proposed MRD-VBAHCHF in handling randomly delayed measurements and contaminated Gaussian noise with unknown statistics.

A. SIMULATION SCENARIO AND PARAMETERS

As shown in Fig. 4 and Fig. 5, a model of the target asteroid Kleopatra was constructed as a polyhedron based on data

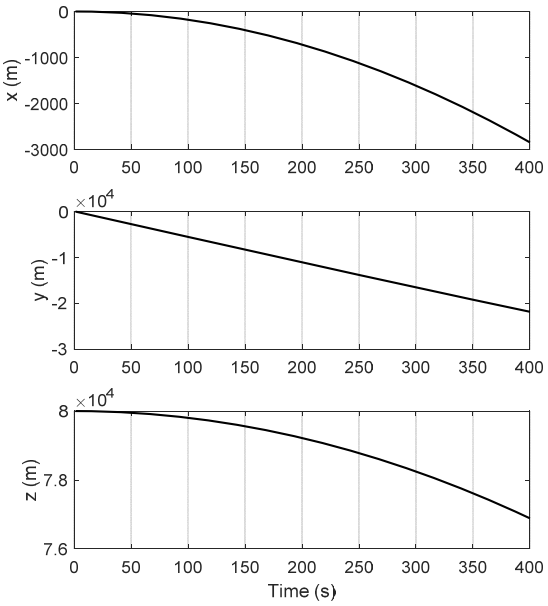

FIGURE 5. The prospector trajectory.

TABLE 1. Simulation parameters.

Parameter	Parameter value
sampling interval	$\Delta t = 1\,\mathrm{s}$
accelerometer bias	$b_a = 0.2\,\mathrm{mg}$
accelerometer random walk	$\nabla_u = 0.002\,\mathrm{mg/s^{1/2}}$
accelerometer white noise	$\nabla_v = 0.02\,\mathrm{mg \cdot s^{1/2}}$
gyro bias	$b_g = 0.1\,\mathrm{deg/h}$
gyro random walk	$\varepsilon_u = 0.06\,\mathrm{deg/h^{3/2}}$
gyro white noise	$\varepsilon_v = 0.01\,\mathrm{deg/h^{1/2}}$
initial position error	$[20\ 20\ 20]\,\mathrm{m}$
initial velocity error	$[2\ 2\ 2]\,\mathrm{m/s}$
initial attitude error	$[0.1\ 0.1\ 0.1]\,\mathrm{deg}$
delay probability	$p_d = 0.1$
perturbing parameter	$\alpha = 0.2$
tuning parameter	$\beta = 1.345$
discount factor	$\kappa = 0.96$
Gaussian-Newton iteration times	$N_{GN} = 3$

from the NASA planetary data system [34]. A "polar" orbit was simulated for 400 s, with an initial position of $\boldsymbol{R}_a = [0, 0, 8.0 \times 10^4]^T m$, an attitude of $\boldsymbol{\Psi} = [0, 0, 0] deg$ and a velocity of $\boldsymbol{V}_a = [0, -55.89, 0] m/s$, and 1250 points were randomly generated to simulate landmarks. The simulation parameters are listed in Table 1. The visual measurements were randomly delayed by at most three steps, with the following delay parameters [22]:

$$p^{(0,j)} = 1 - p_d,\ p^{(1,j)} = \frac{p_d}{2},\ p^{(2,j)} = \frac{p_d}{4},\ p^{(3,j)} = \frac{p_d}{4} \tag{90}$$

where p_d is the delay probability given in Table 1.

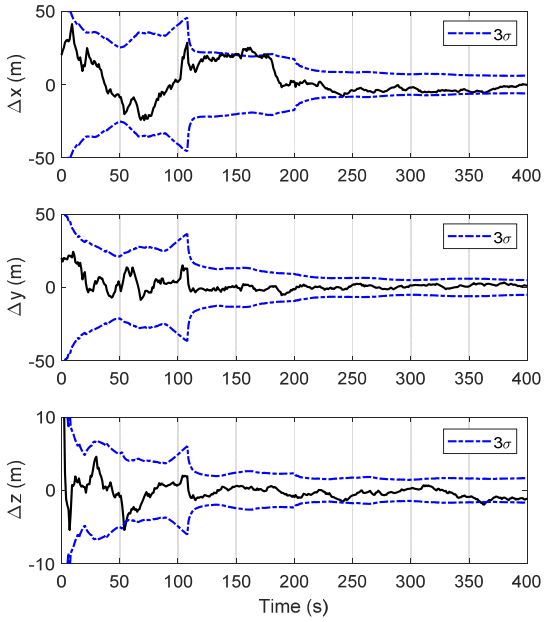

FIGURE 6. Position error of the MRD-VBAHCHF.

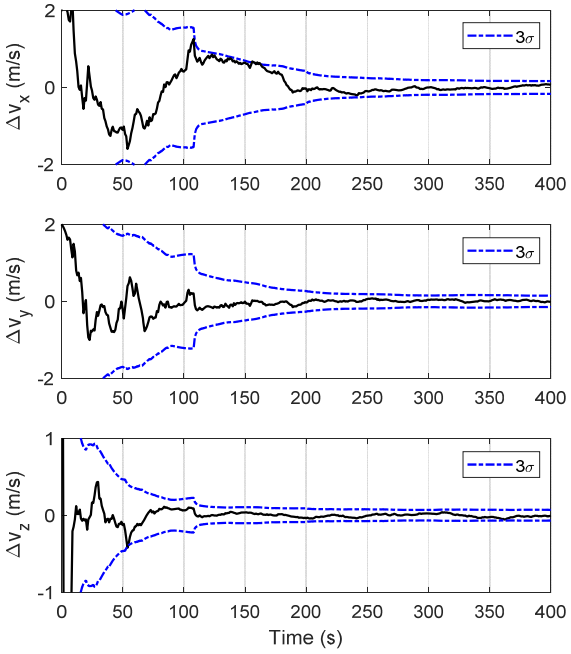

FIGURE 7. Velocity error of the MRD-VBAHCHF.

The contaminated Gaussian measurement noise was drawn from the distribution given in (7), with the following covariances of the ideal Gaussian distribution and the perturbing Gaussian distribution [5]:

$$\boldsymbol{R}_{sen} = \begin{bmatrix} 1.69\times10^{-10} & 0 & 0 \\ 0 & 1.69\times10^{-10} & 0 \\ 0 & 0 & 1.69\times10^{-12} \end{bmatrix} \tag{91}$$

$$\boldsymbol{R}_{per} = 36\boldsymbol{R}_{sen} \tag{92}$$

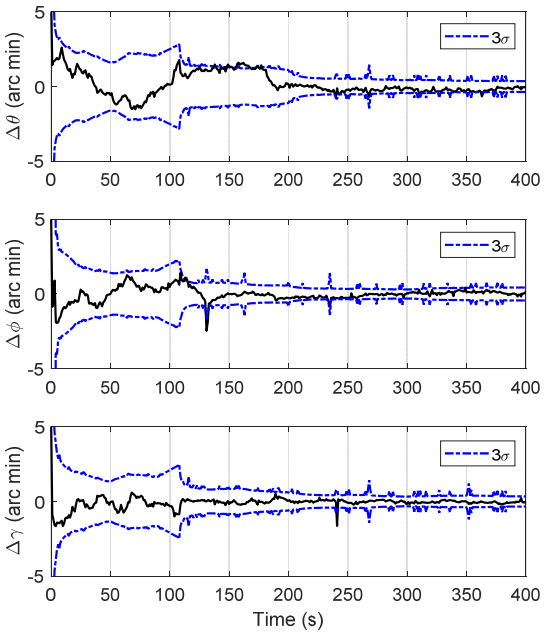

FIGURE 8. Attitude error of the MRD-VBAHCHF.

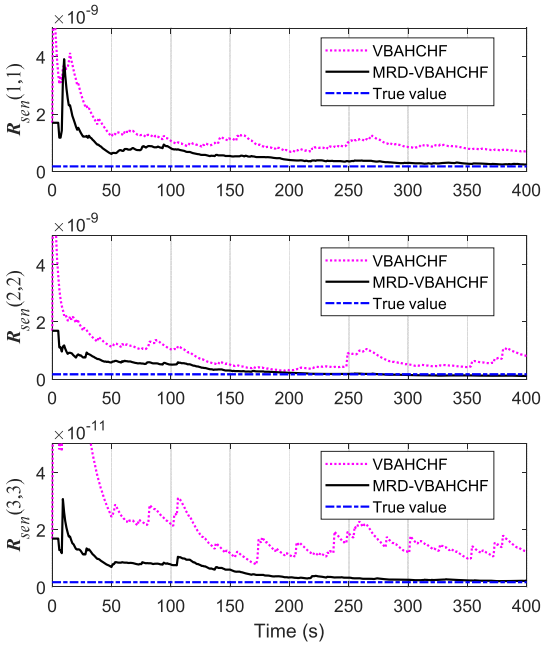

FIGURE 9. Diagonal values of user R_{sen} estimated using the VBAHCHF and MRD-VBAHCHF.

Considering a lack of a priori knowledge of the visual measurement noise, the measurement noise covariance matrices $\boldsymbol{R}_k$ of the HCKF and MRD-HCKF were set as shown in (93). In the variational Bayesian adaptive high-degree cubature Huber-based filter (VBAHCHF) and MRD-VBAHCHF, the initial degree-of-freedom parameter $\hat{u}_{0/0}$ and the scale matrix $\hat{\boldsymbol{U}}_{0/0}$ were set to 11 and $(\hat{u}_{0/0}-m-1)\boldsymbol{R}_0$, respectively.

$$\begin{aligned}\boldsymbol{R}_k = diag([&1.69\times10^{-9}, 1.69\times10^{-9}, 1.69\times10^{-11}, \\ &1.69\times10^{-9}, 1.69\times10^{-9}, 1.69\times10^{-11}, 1.69\times10^{-9}, \\ &1.69\times10^{-9}, 1.69\times10^{-11}])\end{aligned} \tag{93}$$

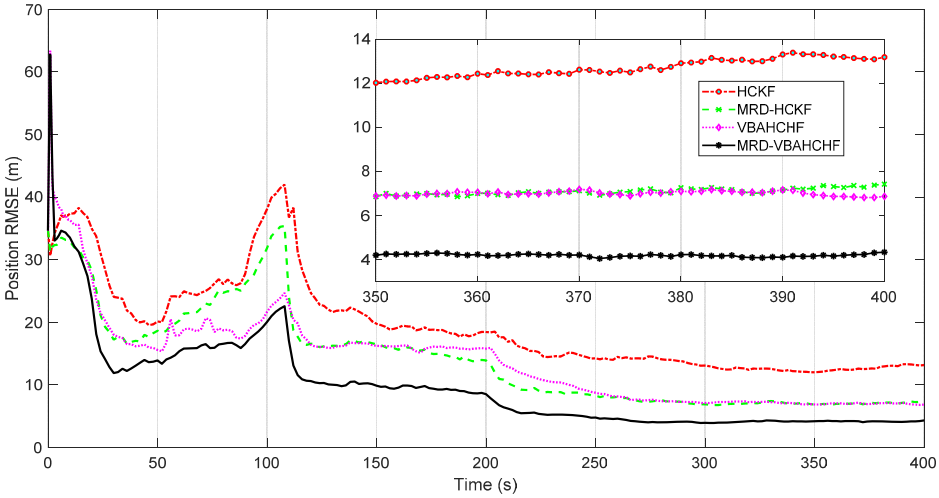

FIGURE 10. Position RMSEs of the HCKF, MRD-HCKF, VBAHCHF and MRD-VBAHCHF.

The process noise covariance matrices $\boldsymbol{Q}_{k-1}$ of the MRD-VBAHCHF and the other filters considered for comparison were chosen in accordance with the statistical characteristics of the inertial measurement unit noise.

$$\begin{aligned}&\boldsymbol{Q}_{k-1}\\&= \mathrm{diag}([10^{-6}, 10^{-6}, 10^{-6}, 1.38\times10^{-6}, 1.38\times10^{-6},\\&\quad 1.38\times10^{-6}, 8.46\times10^{-12}, 8.46\times10^{-12}, 8.46\times10^{-12},\\&\quad 9.62\times10^{-11}, 9.62\times10^{-11}, 9.62\times10^{-11}, 2.35\times10^{-15},\\&\quad 2.35\times10^{-15}, 2.35\times10^{-15}]) \qquad (94)\end{aligned}$$

The initial values of the state $\boldsymbol{x}_{0/0}$ and the covariance $\boldsymbol{P}^{xx}_{0,0/0}$ were set as follows:

$$\begin{aligned}\boldsymbol{x}_{0/0} &= [20, 20, 80020, 2, -53.89, 2, 1.75\times10^{-3},\\&\quad 1.75\times10^{-3}, 1.75\times10^{-3}, 0, 0, 0, 0, 0, 0]^T \qquad (95)\\\boldsymbol{P}^{xx}_{0,0/0} &= \mathrm{diag}([400, 400, 225, 4, 4, 4, 5\times10^{-5},\\&\quad 5\times10^{-5}, 5\times10^{-5}, 1\times10^{-3}, 1\times10^{-3},\\&\quad 1\times10^{-3}, 1\times10^{-6}, 1\times10^{-6}, 1\times10^{-6}]) \qquad (96)\end{aligned}$$

B. SIMULATION RESULTS AND ANALYSES

The proposed filter and the filters considered for comparison were coded in Visual Studio 2005, and the simulations were run on a laptop with an Intel Core i5-2410M CPU @2.30 GHz. The position, velocity and attitude errors of the MRD-VBAHCHF are shown in Figs. 6-8, respectively. The estimation error curves converge rapidly to the 3σ bounds denoted by the blue dash-dotted lines, demonstrating that the proposed filter shows good consistency and accuracy. The diagonal values of $\boldsymbol{R}_{sen}$ estimated using the VBAHCHF and MRD-VBAHCHF are illustrated in Fig. 9. The results suggest that the MRD-VBAHCHF exhibits better performance in estimating the unknown covariance $\boldsymbol{R}_{sen}$ than the VBAHCHF does because the proposed filter considers the random measurement delay, and this means that the MRD-VBAHCHF has better adaptivity than the VBAHCHF. While the HCKF and MRD-HCKF lack of adaptivity because there isn't covariance estimation process in them.

TABLE 2. Comparison of the ARMSEs of the different filtering algorithms.

Filtering algorithm	Position (m)	Velocity (m/s)	Attitude (arc min)
HCKF	19.62	0.59	1.35
MRD-HCKF	14.30	0.52	1.00
VBAHCHF	14.00	0.55	1.13
MRD-VBAHCHF	9.88	0.45	0.79

To quantitatively describe the navigation accuracy, the root mean square errors (RMSEs) of position, velocity and attitude from 100 independent Monte Carlo simulations obtained using the HCKF, MRD-HCKF, VBAHCHF and MRD-VBAHCHF are shown in Figs. 10-12, respectively, and the average RMSEs (ARMSEs) of the four filtering algorithms are presented in Table 2 for comparison. The MRD-VBAHCHF behaves the best, the HCKF behaves the worst, and the MRD-HCKF and VBAHCHF show similar behavior. This is because the MRD-HCKF can address measurements with multiple-step random delays and the VBAHCHF can limit the impact of non-Gaussian noise and estimate the unknown noise covariance, while the MRD-VBAHCHF is capable of handling both multiple-step randomly delayed measurements and contaminated Gaussian measurement noise with unknown statistics. In addition, the single computation time of these four filters are summarized in Table 3. It can be seen that the single computation time of the proposed MRD-VBAHCHF is greater than HCKF, VBAHCHF and MRD-HCKF, but still much less than the sampling interval. So the proposed filter can satisfy the real-time requirement of INS/VNS system.

To further illustrate the filtering performance of the MRD-VBAHCHF under different levels of delay and contamination, additional simulations were implemented by varying

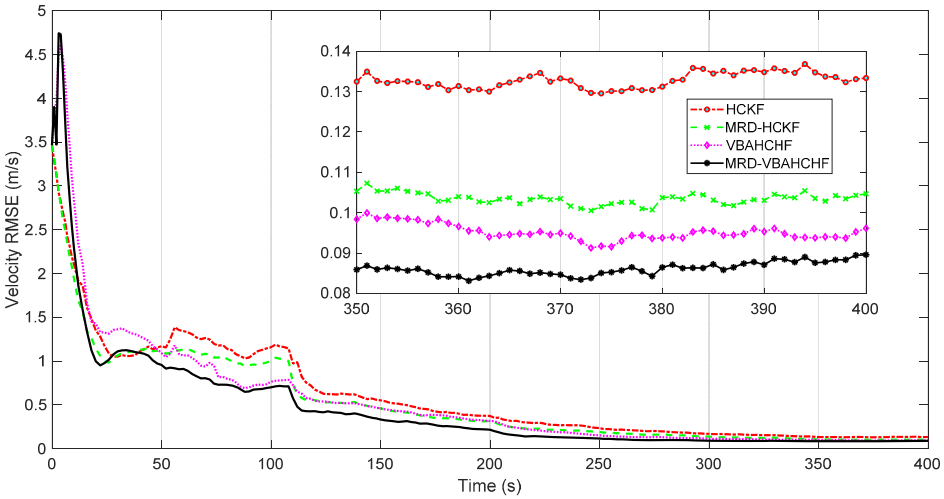

FIGURE 11. Velocity RMSEs of the HCKF, MRD-HCKF, VBAHCHF and MRD-VBAHCHF.

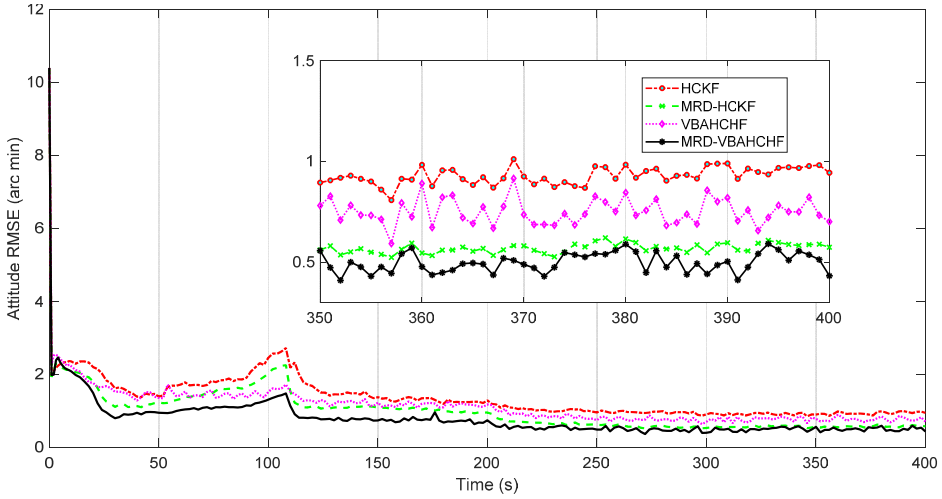

FIGURE 12. Attitude RMSEs of the HCKF, MRD-HCKF, VBAHCHF and MRD-VBAHCHF.

TABLE 3. Single computation time of the different filtering algorithms.

Filtering algorithm	Single computation time (ms)
HCKF	0.71
MRD-HCKF	65.45
VBAHCHF	1.56
MRD-VBAHCHF	78.88

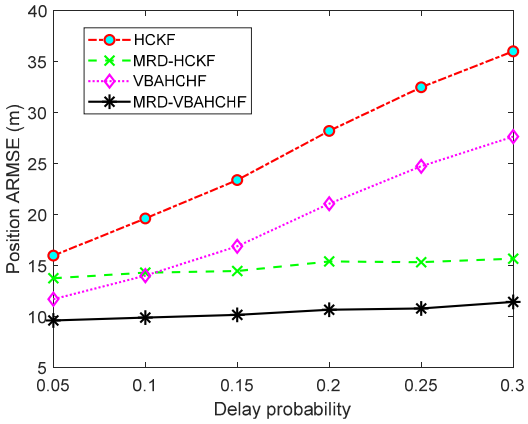

FIGURE 13. Position ARMSEs of the four filtering algorithms under different delay probabilities.

either the delay probability or the perturbing parameter while keeping the other fixed. The corresponding ARMSEs from 100 independent Monte Carlo simulations are presented as follows.

The relationships between the estimation errors of the four filtering algorithms and the delay probability are shown in Figs. 13-15. It is clear that the performance of the HCKF and VBAHCHF decreases rapidly as the delay probability increases. By contrast, the MRD-HCKF and MRD-VBAHCHF show greater robustness to random measurement delay. This is because the MRD-HCKF and MRD-VBAHCHF are derived based on a randomly delayed measurement model. Moreover, the navigation error achieved

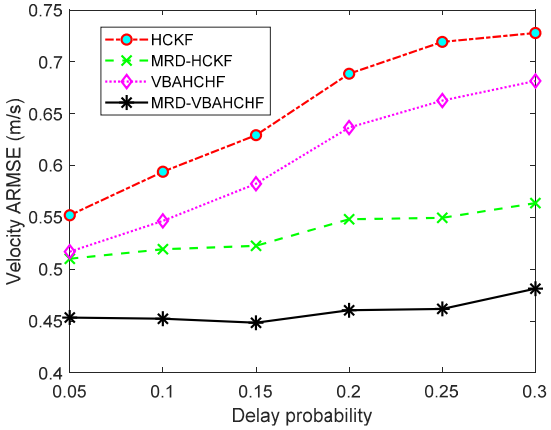

FIGURE 14. Velocity ARMSEs of the four filtering algorithms under different delay probabilities.

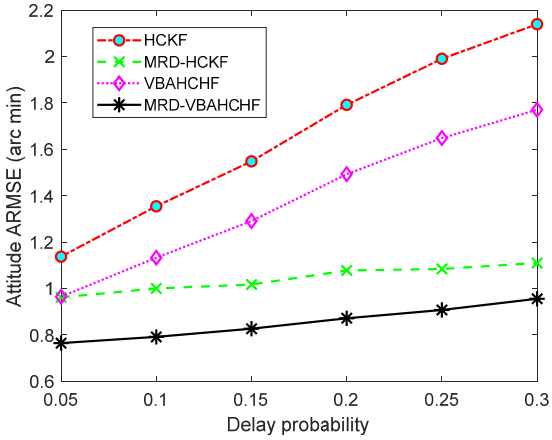

FIGURE 15. Attitude ARMSEs of the four filtering algorithms under different delay probabilities.

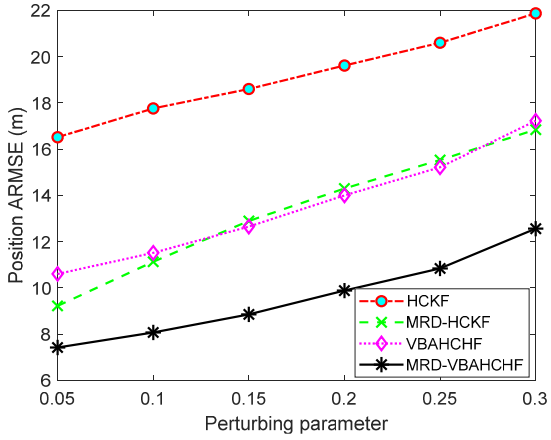

FIGURE 16. Position ARMSEs of the four filtering algorithms under different perturbing parameters.

by the MRD-VBAHCHF is always the smallest under different delay probabilities.

The position, velocity and attitude ARMSEs of the HCKF, MRD-HCKF, VBAHCHF and MRD-VBAHCHF under different perturbing parameters are summarized in Figs. 16-18, respectively. The results show that the estimation errors

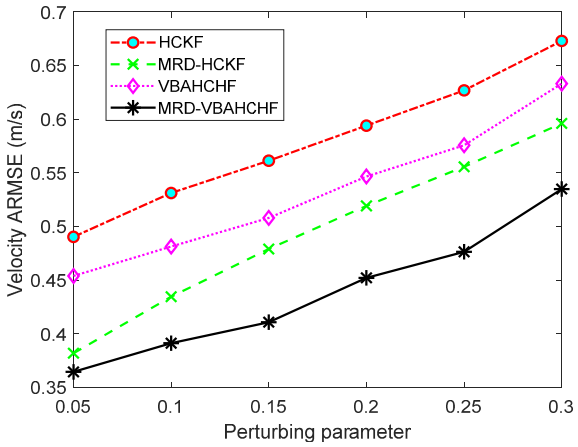

FIGURE 17. Velocity ARMSEs of the four filtering algorithms under different perturbing parameters.

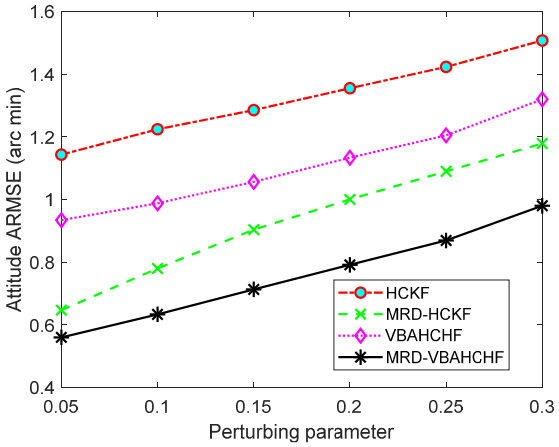

FIGURE 18. Attitude ARMSEs of the four filtering algorithms under different perturbing parameters.

of the VBAHCHF and MRD-VBAHCHF are smaller than those of the HCKF and MRD-HCKF, respectively, thus demonstrating the robustness of the VBAHCHF and MRD-VBAHCHF to contaminated Gaussian noise. These findings are attributed to the fact that the update processes of the VBAHCHF and MRD-VBAHCHF are derived on the basis of the Huber technique and therefore can down weight measurements corrupted by perturbing noise. Furthermore, the MRD-VBAHCHF achieves the highest estimation accuracy under all perturbing parameters.

From the above simulation results, we can conclude that the MRD-VBAHCHF exhibits stronger adaptivity to unknown measurement noise statistics and robustness against random measurement delay and non-Gaussian noise, thereby clearly confirming the superiority of the proposed filtering algorithm.

VII. CONCLUSION

In this article, a novel multiple-step randomly delayed adaptive robust filter called the MRD-VBAHCHF is proposed to handle randomly delayed measurements and contaminated Gaussian measurement noise with unknown covariance, and

its application in INS/VNS integrated navigation for asteroid missions is investigated. First, the MRD-HCKF is derived based on a multiple-step randomly delayed system model and the fifth-degree cubature rule. To estimate the measurement noise covariance online and suppress the influence of non-Gaussian noise, the MRD-HCKF is then combined with the VB theory and Huber technique to develop the MRD-VBAHCHF. Simulation results illustrate that the proposed filtering algorithm achieves the highest estimation accuracy among all filters considered for comparison when simultaneously faced with randomly delayed measurements, contaminated Gaussian noise and unknown measurement noise statistics, thus showing better adaptivity and robustness than the HCKF, MRD-HCKF or VBAHCHF.

REFERENCES

[1] B. Barshan and H. F. Durrant-Whyte, "Inertial navigation systems for mobile robots," *IEEE Trans. Robot. Autom.*, vol. 11, no. 3, pp. 328–342, Jun. 1995.

[2] Y. Tian and M. Yu, "A novel crater recognition based visual navigation approach for asteroid precise pin-point landing," *Aerosp. Sci. Technol.*, vol. 70, pp. 1–9, Nov. 2017.

[3] M. Yu, S. Li, S. Wang, and X. Huang, "Single crater-aided inertial navigation for autonomous asteroid landing," *Adv. Space Res.*, vol. 63, no. 2, pp. 1085–1099, Jan. 2019.

[4] X. Ning, M. Gui, J. Zhang, and J. Fang, "A dimension reduced INS/VNS integrated navigation method for planetary rovers," *Chin. J. Aeronaut.*, vol. 29, no. 6, pp. 1695–1708, Dec. 2016.

[5] B. Razgus, E. Mooij, and D. Choukroun, "Relative navigation in asteroid missions using dual quaternion filtering," *J. Guid., Control, Dyn.*, vol. 40, no. 9, pp. 2151–2166, Sep. 2017.

[6] D. Ji, Z. Deng, S. Li, D. Ma, T. Wang, W. Song, S. Zhu, Z. Wang, H. Pan, S. Sharma, and X. Yang, "A novel case of practical exponential observer using extended Kalman filter," *IEEE Access*, vol. 6, pp. 58004–58011, Sep. 2018.

[7] S. Julier, J. Uhlmann, and H. F. Durrant-Whyte, "A new method for the nonlinear transformation of means and covariances in filters and estimators," *IEEE Trans. Autom. Control*, vol. 45, no. 3, pp. 477–482, Mar. 2000.

[8] J. Yin, R. Tiwari, and M. Johnston, "Robust GPS carrier tracking model using unscented Kalman filter for a dynamic vehicular communication channel," *IEEE Access*, vol. 6, pp. 26930–26938, May 2018.

[9] I. Arasaratnam and S. Haykin, "Cubature Kalman filters," *IEEE Trans. Autom. Control*, vol. 54, no. 6, pp. 1254–1269, Jun. 2009.

[10] H. Huang, J. Zhou, J. Zhang, Y. Yang, R. Song, J. Chen, and J. Zhang, "Attitude estimation fusing quasi-Newton and cubature Kalman filtering for inertial navigation system aided with magnetic sensors," *IEEE Access*, vol. 6, pp. 28755–28767, May 2018.

[11] K. Ito and K. Xiong, "Gaussian filters for nonlinear filtering problems," *IEEE Trans. Autom. Control*, vol. 45, no. 5, pp. 910–927, May 2000.

[12] B. Jia and M. Xin, "Multiple sensor estimation using a new fifth-degree cubature information filter," *Trans. Inst. Meas. Control*, vol. 37, no. 1, pp. 15–24, Jan. 2015.

[13] B. Jia, M. Xin, and Y. Cheng, "High-degree cubature Kalman filter," *Automatica*, vol. 49, no. 2, pp. 510–518, Feb. 2013.

[14] R. Esmzad and R. Mahboobi Esfanjani, "Modified likelihood probabilistic data association filter for tracking systems with delayed and lost measurements," *Digit. Signal Process.*, vol. 76, pp. 66–74, May 2018.

[15] L. Chang, B. Hu, G. Chang, and A. Li, "Huber-based novel robust unscented Kalman filter," *IET Sci. Meas. Technol.*, vol. 6, no. 6, pp. 502–509, Nov. 2012.

[16] H. Xu, H. Yuan, K. Duan, W. Xie, and Y. Wang, "Adaptive high-degree cubature Kalman filter in the presence of unknown measurement noise covariance matrix," *J. Eng.*, vol. 2019, no. 19, pp. 5697–5701, Oct. 2019.

[17] C. Yang, A. Soloviev, M. Veth, and C. Taylor, "Vision-aided inertial navigation with modeling of measurement outliers," *J. Aerosp. Inf. Syst.*, vol. 12, no. 12, pp. 673–687, Dec. 2015.

[18] A. Hermoso-Carazo and J. Linares-Pérez, "Extended and unscented filtering algorithms using one-step randomly delayed observations," *Appl. Math. Comput.*, vol. 190, no. 2, pp. 1375–1393, Jul. 2007.

[19] A. Hermoso-Carazo and J. Linares-Pérez, "Unscented filtering algorithm using two-step randomly delayed observations in nonlinear systems," *Appl. Math. Model.*, vol. 33, no. 9, pp. 3705–3717, Sep. 2009.

[20] R. Caballero-Águila, A. Hermoso-Carazo, and J. Linares-Pérez, "A new estimation algorithm from measurements with multiple-step random delays and packet dropouts," *Math. Problems Eng.*, vol. 2010, pp. 1–18, May 2010.

[21] A. K. Singh, P. Date, and S. Bhaumik, "A modified Bayesian filter for randomly delayed measurements," *IEEE Trans. Autom. Control*, vol. 62, no. 1, pp. 419–424, Jan. 2017.

[22] W. Qin, X. Wang, Y. Bai, and N. Cui, "Arbitrary-step randomly delayed robust filter with application to boost phase tracking," *Acta Astronautica*, vol. 145, pp. 304–318, Apr. 2018.

[23] R. Esmzad and R. M. Esfanjani, "Bayesian filter for nonlinear systems with randomly delayed and lost measurements," *Automatica*, vol. 107, pp. 36–42, Sep. 2019.

[24] P. J. Huber, "Robust estimation of a location parameter," *Ann. Math. Statist.*, vol. 35, no. 1, pp. 73–101, Mar. 1964.

[25] Y. Wang, S. Sun, and L. Li, "Adaptively robust unscented Kalman filter for tracking a maneuvering vehicle," *J. Guid., Control, Dyn.*, vol. 37, no. 5, pp. 1696–1701, Sep. 2014.

[26] P. Petrus, "Robust huber adaptive filter," *IEEE Trans. Signal Process.*, vol. 47, no. 4, pp. 1129–1133, Apr. 1999.

[27] S. Sarkka and J. Hartikainen, "Non-linear noise adaptive Kalman filtering via variational Bayes," in *Proc. IEEE Int. Workshop Mach. Learn. Signal Process. (MLSP)*, Sep. 2013, pp. 22–25.

[28] K. Li, L. Chang, and B. Hu, "A variational Bayesian-based unscented Kalman filter with both adaptivity and robustness," *IEEE Sensors J.*, vol. 16, no. 18, pp. 6966–6976, Sep. 2016.

[29] J. Hou, H. He, Y. Yang, T. Gao, and Y. Zhang, "A variational Bayesian and Huber-based robust square root cubature Kalman filter for lithium-ion battery state of charge estimation," *Energies*, vol. 12, no. 9, pp. 1–23, May 2019.

[30] Y. Huang and Y. Zhang, "Robust student's t-based stochastic cubature filter for nonlinear systems with heavy-tailed process and measurement noises," *IEEE Access*, vol. 5, pp. 7964–7974, May 2017.

[31] S. Challa, M. R. Morelande, D. Mušicki, and R. J. Evans, *Fundamentals of Object Tracking*. Cambridge, U.K.: Cambridge Univ. Press, 2011.

[32] D. Sun and J. L. Crassidis, "Observability analysis of six-degree-of-freedom configuration determination using vector observations," *J. Guid., Control, Dyn.*, vol. 25, no. 6, pp. 1149–1157, Nov. 2002.

[33] Y. B. Park, H. C. Jeon, and C. G. Park, "Analysis of geometric effects on integrated inertial/vision for lunar descent navigation," *J. Guid. Control Dyn.*, vol. 39, no. 4, pp. 935–941, Apr. 2016.

[34] C. E. Neese. (2004). Small body radar shape models V2.0. EAR-A-5-DDR-RADARSHAPE-MODELS-V2.0. NASA Planetary Data System. [Online]. Available: https://sbn.psi.edu/pds/resource/rshape.html

RONGJUN MU received the M.S. degree from Northeast Normal University, Changchun, China, in 2000, and the Ph.D. degree in aeronautical and astronautical science and technology from the Harbin Institute of Technology, Harbin, China, in 2006. He is currently a Professor with the School of Astronautics, Harbin Institute of Technology. He has authored more than 60 papers published in international journals and conference proceedings. His main research interests include space vehicle navigation and filtering theory.

BINGZHI SU received the B.S. degree in flight vehicle design and engineering from the Harbin Institute of Technology, Harbin, China, in 2014, where he is currently pursuing the Ph.D. degree in aeronautical and astronautical science and technology. His main research interests include flight mechanics and nonlinear filtering theory and its applications in navigation technology, such as the initial alignment of inertial navigation systems and integrated navigation.

JIAYE CHEN received the M.S. degree in aerospace engineering and the Ph.D. degree in aeronautical and astronautical science and technology from the Harbin Institute of Technology, Harbin, China, in 2015 and 2019, respectively. He is currently an Engineer with the Beijing Institute of Astronautical Systems Engineering. His main research interests include the modeling of spacecraft dynamics and the attitude control of reusable launch vehicles.

YUNTIAN LI received the M.S. degree in aerospace engineering from the Harbin Institute of Technology, Harbin, China, in 2015, where he is currently pursuing the Ph.D. degree in aeronautical and astronautical science and technology. From 2015 to 2020, he was a joint Ph.D. Student with the Department of Mechanical and Aerospace Engineering, Politecnico di Torino. His main research interests include visual navigation and information fusion.

NAIGANG CUI received the M.S. degree in flight mechanics and the Ph.D. degree in guidance and control and simulation from the Harbin Institute of Technology, Harbin, China, in 1989 and 1996, respectively. He is currently a Professor with the School of Astronautics, Harbin Institute of Technology. His main research interests include nonlinear filtering theory, the guidance of launch vehicles, and flight mechanics. He received the Second Prize for Scientific and Technological Progress from the China's Department of Aeronautics, in 2006.